# Molecular Dynamics Simulation of Antimicrobial Peptide Arenicin-2: β-Hairpin Stabilization by Noncovalent Interactions

Athanassios Stavrakoudis,[1] Ioannis G. Tsoulos,[2] Zakhar O. Shenkarev,[3] Tatiana V. Ovchinnikova[3]

[1]*Department of Economics, University of Ioannina, GR-45110, Ioannina, Greece*

[2]*Department of Computer Science, University of Ioannina, GR-45110, Ioannina, Greece*

[3]*Shemyakin and Ovchinnikov Institute of Bioorganic Chemistry, Russian Academy of Sciences, Miklukho-Maklaya str., 16/10, 117997 Moscow, Russia*

*Received 13 May 2008; revised 23 November 2008; accepted 14 January 2009*
*Published online 2 February 2009 in Wiley InterScience (www.interscience.wiley.com). DOI 10.1002/bip.21149*

## ABSTRACT:

*Arenicin-2 is a 21 residue antimicrobial cyclic peptide, possessing one disulphide bond between residues $Cys_3$ and $Cys_{20}$. NMR and CD studies suggested that the structure of arenicin-2 in water represented a well formed, but highly twisted β-harpin. To investigate the spatial arrangement of the peptide side chains and to get a clear view of its possible amphipathic properties we performed molecular dynamics in explicit water. Four independent trajectories, 50 ns in length, were produced, starting from various initial conformations or by applying different simulation conditions. Arenicin-2 retained its β-hairpin structure during simulations, although the residues close to strand ends were found to escape from the ideal hairpin conformation. The type I′ β-turn connecting the two strands fluctuated between type IV and II′ β-turn. Conversely, the right-handed twist of the β-hairpin was well conserved with average twist value 203° ± 19° per eight residues. Several nonbonded interactions, like hydrophobic interactions between aliphatic side chains, cation/π-aromatic interactions, CH. . .π aromatic bond and water bridges, contributed to the hairpin stabilization. © 2009 Wiley Periodicals, Inc. Biopolymers (Pept Sci) 92: 143–155, 2009.*

*Keywords: β-hairpin; arenicin-2; antimicrobial peptide; cation/π-aromatic interaction; CH-π; aromatic bond; computer simulation; molecular dynamics; peptide structure*

*This article was originally published online as an accepted preprint. The "Published Online" date corresponds to the preprint version. You can request a copy of the preprint by emailing the Biopolymers editorial office at biopolymers@wiley.com*

## INTRODUCTION

It is widely accepted that antimicrobial peptides (AMPs) target the lipid bilayer of the bacterial cell membrane, instead of specific protein receptors within the cell membrane.[1,2] Differences in membrane composition provide a way for AMPs to distinguish between mammalian and bacterial cell membranes. In most cases, antimicrobial peptides carry a positive charge and a substantial portion of hydrophobic residues, and adopt an amphipathic conformation with opposing hydrophobic and positively charged faces when they are in contact with bacterial membranes.[3] A large number of naturally occurred antimicrobial peptides have been isolated and their number is growing year by year. Peptide chemists also contribute to the enlargement of available antimicrobial peptides by designing synthetic ones.[4]

Arenicins are antimicrobial peptides isolated from coelomocytes of marine polychaeta lugworm *Arenicola marina*.[5]

Additional Supporting Information may be found in the online version of this article.

*Correspondence to:* Athanassios Stavrakoudis, Department of Economics, University of Ioannina, GR-45110 Ioannina, Greece; E-mail: astavrak@cc.uoi.gr and Tatiana V. Ovchinnikova, Shemyakin and Ovchinnikov Institute of Bioorganic Chemistry, Russian Academy of Sciences, Miklukho-Maklaya str., 16/10, 117997 Moscow, Russia; E-mail: ovch@ibch.ru

Contract grant sponsor: Russian Foundation for Basic Research.
Contract grant number: 09-04-01202.

Invertebrate animals, living without adaptive immunity in a microbe laden environment, produce AMPs as an important evolutionary conserved component of their innate immune system which plays a key role in the host defense against bacterial, fungal, and viral invasion. Two isoforms have been identified: arenicin-1 (R W C V Y A Y V R V R G V L V R Y R R C W) and arenicin-2 (R W C V Y A Y V R I R G V L V R Y R R C W). $Cys_3$ and $Cys_{20}$ in both arenicins form a disulfide bond forming a 18-residue ring. Arenicins show no sequence similarity to other antimicrobial peptides discovered until now. The solution structure of arenicin-2 has been recently determined by combined NMR and CD study.[6] As found the peptide adopts a highly twisted $\beta$-hairpin conformation stabilized by several backbone hydrogen bonds, as well as by the disulfide bond.

Although the majority of antimicrobial peptides adopt a helical conformation, the number of different conformations increases in the literature that evidences for larger research efforts in this field. Few other AMPs show a $\beta$-hairpin conformation in solution such as thanatin,[7] lactofericin B,[8] RTD-1 defensin,[9] gomesin,[10] tachyplesin I,[11] hepcidin,[12] androctonin[13] and protegrin-1.[14,15] Anyway these peptides (except for thanatin and lactofericin B) have four cysteines in their sequence and possess two disulfide bonds. From this point of view the structure of arnicin-2 is quite rare among antimicrobial peptides. To our knowledge, there is no antimicrobial peptide with the $\beta$-hairpin conformation without a disulfide bridge or any other cyclic structure. Disulfide linkages are well-known stabilizing factors in protein structure[16] and provide an excellent mean for peptide engineering.[17]

In this work, we present the molecular dynamics (MD) studies or arenicin-2 in solution starting from the NMR-solved structure. The aim of the study is to provide a high-resolution atomistic view of specific interactions that cannot be easily captured by experimental techniques[18] because of space or/and time averages. Such complementary investigations proved to enlighten our knowledge of peptide/protein structural properties[19] and to help better understanding of their action.[20] One of the main targets of this study was to explore possible interactions among arginine and aromatic residues side chains. These type of residues occupy almost 50% of the arenicin primary structure, their interactions are expected to play a crucial role in its structure and activity, as it was found in other similar cases.[21] Aromatic/arginine residue side chain stacking was supposed to play also an important role in protein–protein interactions[22,23] and antimicrobial peptides activity.[21] On the basis of the obtained MD trace, the highly twisted $\beta$-hairpin structure of arenicin-2 is explored that yielded valuable information. Atomistic computational simulations can provide a framework for detailed analysis of such specific interactions and contribute to our knowledge of peptide folding[19] and antimicrobial activity.

**Table I Simulation Set Up Details About the Four Presented MD Trajectories**

| Trajectory | Starting Model[a] | Temperature (K) | Cutoff (nm) |
|---|---|---|---|
| M1 | 1 | 288 | 0.12 |
| M3 | 3 | 288 | 0.12 |
| 310K | 1 | 310 | 0.12 |
| c14 | 1 | 288 | 0.14 |

[a] Starting model from the NMR bundle of structures as deposited at PDB (entry code 2JNI).

## MATERIALS AND METHODS

Four independent MD trajectories were produced, details are shown in the Table I. Initial peptide coordinates were extracted from the arenicin-2 NMR structure as deposited at PDB, access code 2JNI.[6] Starting conformation was built from the first model of NMR-derived bundle of structures using the VMD program.[24] The peptide was solvated with TIP3P[25] water molecules using a rectangular box with dimensions $7.23 \times 5.31 \times 5.46$ nm$^3$. This allowed a distance of at least 1.8 nm between any peptide atom and the edges of the box to avoid simulation artifacts.[26] The system was neutralized by placing 12 $Na^+$ and 18 $Cl^-$ ions using VMD solvate and autoionize plugins. This system was used as starting point for three independent trajectories: M1, 310K, and c14 (Table I). The fourth trajectory (M3) was produced by using the 3rd model structure from the NMR bundle. This conformation was used because it showed the biggest backbone RMSD from the 1st model. Topology and force field parameters for all atoms were assigned from the CHARMM27 parameter set.[27] So, all subsequent MM and MD runs were performed with the NAMD[28] program (v2.6) using 12 CPUs of a Linux cluster. Nonbonded van der Waals interactions were gradually turned off at the distance between 1.0 and 1.2 nm for M1, M3, and 310K cases and between 1.2 and 1.4 nm for the c14 case. The nonbonded pair list was updated every 10 steps. Long range electrostatics were computed every step by the PME method,[29] with a grid spacing of less than 0.1 nm. The bonds to hydrogen atoms were constrained with the SHAKE[30] with a relative tolerance of $10^{-8}$, allowing a 2-fs step during subsequent MD runs. The whole system was energy minimized with 2500 conjugate gradient steps. After energy minimization the temperature of the system gradually increased with Langevin dynamics, using the NVT ensemble, to 288 K (310 K for the 310K trajectory), during the period of 3000 steps, by stepwise reassignment of velocities every 500 steps. At this stage, heavy atoms of the peptide model were restrained to their initial positions with a force constant of 50 kcal mol$^{-1}$ Å$^{-2}$. The simulation continued until 100,000 steps (0.2 ns). The force constant of positional restraints was then decreased to 5 kcal mol$^{-1}$ Å$^{-2}$ for other 100,000 steps and finally positional restraints were totally eliminated for subsequent 200,000 steps of NVT equilibration period. The simulation continued under constant pressure, with the Langevin piston method,[31] thus NPT ensemble, for 50 ns. Pressure was maintained at 1 atm and the temperature was kept at 288 K

(310 K for the 310K trajectory). The results presented here are from this, isothermal–isobaric ensemble, MD run. Snapshots were saved to disk at 1-ps interval for further analysis.

Conformation analysis and visual inspection of the structures were performed with VMD[24] and Carma[32] software packages, along with some in-house Mathematica and C++ code (http://stavrakoudis.econ.uoi.gr/eucb/). Secondary structure assignment was performed with STRIDE.[33] Structural figures were prepared with PYMOL.[34]

The values of $^3J(H^{\alpha}\text{-}H^{N})$ coupling constants were computed using Karplus equation

$$^3J = a\cos^2(\phi - 60) + b\cos(\phi - 60) + c \quad (1)$$

where $a = 6.98$, $b = -1.38$, and $c = 1.72$.[35] $^3J$ values were obtained for every frame of a trajectory and average values were calculated. Average square distance between experimental[6] and theoretical values were measured as:

$$R_{3J} = \sqrt{\frac{1}{N}\sum_{i=1}^{N}\left(J_{\text{exp}} - J_{\text{theor}}\right)^2} \quad (2)$$

Averaged distances between $H^{\alpha}$, $H^{N}$, and $H^{\beta}$ atoms were computed by the formula

$$d_{ij} = \left\langle r_{ij}^{-1/6} \right\rangle^{1/6} \quad (3)$$

where $r_{ij}$ is the Euclidean distance between atoms $i$ and $j$, measured from Cartesian coordinates of trajectory frames.

To measure the stacking between the planar side chains of arginine, tyrosine or tryptophan residues we used a simple procedure by calculating the distance and angle between planes defined by each side chain. The atoms used to define each plane equation were $N^{\varepsilon}$, $N^{\eta 1}$, $N^{\eta 2}$ for arginine, $C^{\gamma}$, $C^{\varepsilon 1}$, $C^{\varepsilon 2}$ for tyrosine and $C^{\delta 1}$, $C^{\varepsilon 3}$, $C^{\zeta 2}$ for tryptophan side chains, respectively. The distance between two planar groups was calculated as Euclidean distance between averaged coordinates of the three atoms. We adopted a 0.6 nm distance cutoff as a criterion of the proximity of two planar side chains. The angle between two planar groups was also calculated. Since an angle sign is not to matter a bit, in our study we used the transformation $\alpha = \min(\text{abs}(\alpha), 180\text{-abs}(\alpha))$ for calculated angle $\alpha$, and we used a three state model to describe a parallel or perpendicular orientation of two groups. Planar side chains were classified to be (a) in parallel orientation if the angle was found less than 30°, (b) in perpendicular orientation if the angle was found bigger than 60°, and (c) not classified in other cases.

To evaluate T-shaped aromatic/arginine interactions,[36] the distance between any of the nitrogen atoms of side chain of arginine ($N^{\varepsilon}$, $N^{\eta 1}$, $N^{\eta 2}$) residue and the center of an aromatic ring was measured, along with the angle between the N—H vector and the aromatic plane defined by three atoms as previously mentioned. We adopted a single geometrical criterion for defining a vertical (T-shaped) interaction: the distance to be less than 0.45 nm and the angle to be less than 30°, to accept a T-shaped arginine/aromatic interaction.

The overall geometry of the $\beta$-hairpin in the terms of "kink" and "twist" angles was analyzed at 10-ps intervals of the simulation (for each the 10th frame of the saved MD trajectory). The geometric values were calculated using coordinates of backbone $N^{H}$ and C′ atoms of the peptide. The $C^{\alpha}$ atoms were excluded from the analysis because of well-described "pleated" nature of $\beta$-sheets with $C^{\alpha}$ atoms projected from the sheet plane.[37] The "kink" was defined as a cross-angle between two vectors $a$ and $b$, where $a$ is a mean of the $Ala_6$:C′-$Trp_2$:C′ and $Tyr_{17}$:$N^{H}$-$Trp_{21}$:$N^{H}$ vectors, and $b$ is a mean of the $Ala_6$:C′-$Ile_{:10}$C′ and $Tyr_{17}$:$N^{H}$-$Val_{13}$:$N^{H}$ vectors. The "twist" was defined as a cross-angle between two vectors $Trp_2$:C′-$Trp_{21}$:$N^{H}$ and $Ile_{10}$:C′-$Val_{13}$:$N^{H}$.

The shortest distance between side chain carbon atoms of residues with aliphatic side chains (Val, Ile) was used for the evaluation of their hydrophobic interaction.

## RESULTS AND DISCUSSION

### Backbone Conformation and Overall Peptide Structure

Figure 1A shows the RMSF of backbone $C^{\alpha}$ atoms of arenicin-2 from the four MD trajectories. RMSF plot shows the same profile, thus the mobility of the peptide backbone was not influenced significantly from the application of different simulation conditions. As expected, N- and C-terminal residues, lying outside the disulfide loop, showed increased

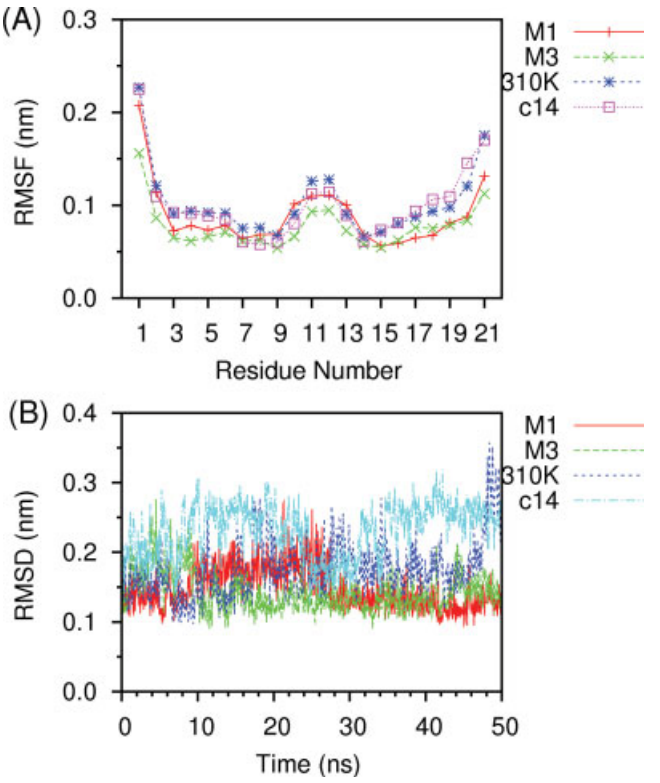


**FIGURE 1** A) Root Mean Square Fluctuation (RMSF) of $C^{\alpha}$ atoms in the four MD trajectories. (B) Time evolution of RMSD of backbone atoms over the corresponding starting conformation of each MD trajectory.

**Table II Conformational Clusters (Assigned by STRIDE) Based on Secondary Structure Assignment Observed in the Four MD Trajectories**

| Sequence/Structure | % Occurrence | | | |
|---|---|---|---|---|
| WCVYAYVRIRGVLVRYRRC | M1 | M3 | 310K | c14 |
| CCCEEEEEETTEEEEECC | | | 10.6 | 34.6 |
| CCEEEEEEETTEEEEEEC | 11.9 | 58.1 | 70.8 | 52.9 |
| CCEEEEEETTTCEEEEEC | 42.3 | | | |
| CCEEEEEETTTTEEEEEC | 12.2 | | | |
| CCEEEEEETTTTEEEEEC | | 5.7 | 9.8 | 6.7 |
| CCEEEEETTTTCCEEEEEC | 5.8 | | | |
| CEEEEEEEETTEEEEEEEE | | 26.4 | | |
| CEEEEEEETTTCEEEEEEE | 15.3 | | | |

Residues $Arg_1$ and $Trp_{21}$ (N- and C-terminal respectively) were excluded from calculations.

mobility with RMSF values around 0.2 nm. According to $C^{\alpha}$'s RMSF calculations peptide edges showed increased mobility as indicated with relative big values, especially for $Arg_1$ residue (RMSF > 0.2 nm). The residues adjacent to cysteines and located out of the hairpin loop, $Trp_2$ and $Trp_{21}$, had also relatively big values ($\sim$0.2 nm). Residues that had strand conformation, $Cys_3$-$Arg_9$ and $Ile1_{14}$-$Cys_{20}$ showed the minimal $C^{\alpha}$ fluctuations with RMSF values of 0.07–0.09 nm. Interestingly, the $\beta$-turn residues $Ile_{10}$-$Val_{13}$ showed a higher mobility and RMSF values were found 0.12–0.13 nm. RMSF plot shows a weak peak at $Arg_{11}$-$Gly_{12}$ residues with the values ranging from $\sim$0.1 nm (M3) to $\sim$0.14 nm (310K). Time evolution of RMSD calculated from the four MD trajectories is shown in Figure 1B. The great majority of trajectory recorded values between 0.1 and 0.3 nm in all the four cases. Increased temperature at 310K trajectory did not seem to influence the mobility of the backbone atoms, as the recorded RMSD values of the 310K and M1, M3 trajectories did not differ significantly. The application of a bigger cutoff (0.14 nm) of nonbonded interactions (c14 trajectory) had moderate effect on RMSD values. Applying a too short cutoff at MD simulations is a well-known source of severe problems. Moreover, recent studies have shown that a bigger cutoff (1.4 nm for example) might also lead to problematic MD results.[36] The c14 MD trajectory showed bigger RMSD values form the other three MD trajectories, even from the 310K. That is somewhat unusual, since increasing the temperature is expected to influence the mobility of the peptide in a greater extent than applying a bigger cutoff. These result are in line with recent work indicating the optimal nonbonded cutoff value to be 0.12 nm.[36]

Table II summarizes the conformational clusters observed in the four MD trajectories (time series of secondary structure assignment can be found in the supporting information). Representative structures from the four MD trajectories are also shown in Figure 2. Considering the secondary structure of individual residues, only minor dissimilarities between NMR and MD data were found. Peptide residues $Val_4$-$Arg_9$ and $Ile1_4$-$Arg_{19}$ were found to be in $\beta$-strand conformation. Residues located at the edges of the peptide sequence, $Arg_1$-$Cys_3$ and $Cys_{20}$-$Trp_{21}$, residues were found in coil conformation. It is worthy to note that $Cys_3$ and $Cys_{20}$ were found at strand conformation in NMR bundle of structures. The residues $Arg_{11}$-$Gly_{12}$ retained turn conformation although altered turn types were observed during MD trajectory. In the M1 trajectory there was a minor conformational transition around 7 ns of the simulation time. Average $\varphi_{10}$ value of $-135^{\circ}$ from NMR data shifted to $-96^{\circ}$ as averaged from MD time series. Dihedral angle $\psi_{10}$ showed a transition from $100^{\circ}$ to $-63^{\circ}$ at about 7 ns of the simulation time where the average value from NMR data was $132^{\circ}$. Concurrently, $\varphi_{11}$ experienced a similar transition from $62^{\circ}$ to $-103^{\circ}$.

The $\varphi_{11}$ transition observed during M1 trajectory resulted in a significantly greater $^3J$ ($H^N$-$H^{\alpha}$) coupling constant (calculated from the MD data) that corresponds to the $\varphi_{11}$ dihedral angle ($Arg_{11}$ $H^N$ and $H^{\alpha}$ atoms). The experimental (NMR) value was found to be 4.9 Hz, while the calculated values were found to be 8.9 Hz for the M1 trajectory and 7.1 Hz for the M3, 310K, c14 trajectories (Table III). This fact indicates that $\varphi_{11}$ transition was probably a simulation artifact and that MD trajectories M3, 310K, and c14 reproduced the NMR data in a more consistent level.

The transitions of backbone dihedrals (M1 trajectory) disrupted the $\beta$-turn conformation of the $Ile_{10}$-$Val_{13}$ fragment that connected the two $\beta$-strands but did not alter its bend configuration that could lead to subsequent unfolding of the

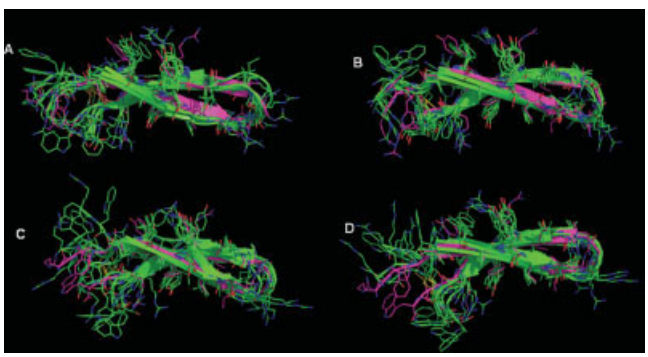


**FIGURE 2** Superimposition of backbone atoms of five conformations (every 10 ns) on their starting conformation (from NMR data, colored magenta) of the (A) M1 (B) M3, (C) 310K, and (D) c14 trajectories. Backbone atoms are also shown in ribbons. Hydrogen atoms were removed for the clarity of representation.

**Table III Experimental (from Ref. 6) and Simulated $^3J$ ($H^{\alpha}$-$H^{N}$) Coupling Constants (See Methods) of Arenicin-2**

| | | MD | | | |
|---|---|---|---|---|---|
| Residue | NMR | M1 | M3 | 310K | c14 |
| $Trp_2$ | 8.30 | 7.83 | 7.74 | 8.12 | 8.47 |
| $Cys_3$ | 9.35 | 8.00 | 8.11 | 8.02 | 7.57 |
| $Val_4$ | 8.60 | 9.41 | 9.02 | 8.64 | 7.41 |
| $Tyr_5$ | 9.00 | 8.63 | 8.45 | 8.17 | 7.57 |
| $Ala_6$ | 8.90 | 8.93 | 9.06 | 9.11 | 9.05 |
| $Tyr_7$ | 10.0 | 9.76 | 9.59 | 9.6 | 9.63 |
| $Val_8$ | 8.90 | 9.11 | 9.02 | 9.31 | 9.24 |
| $Arg_9$ | 7.10 | 8.79 | 8.56 | 8.12 | 8.12 |
| $Ile_{10}$ | 9.00 | 8.54 | 9.13 | 9.31 | 9.29 |
| $Arg_{11}$ | 4.90 | 8.88 | 7.14 | 7.12 | 7.14 |
| $Val_{13}$ | 9.20 | 8.36 | 8.97 | 8.69 | 8.85 |
| $Leu_{14}$ | 6.70 | 7.09 | 7.96 | 7.77 | 7.36 |
| $Val_{15}$ | 9.35 | 7.29 | 7.74 | 8.08 | 8.13 |
| $Arg_{16}$ | 7.80 | 9.21 | 9.62 | 9.34 | 9.38 |
| $Tyr_{17}$ | 8.50 | 8.11 | 8.77 | 8.18 | 8.56 |
| $Arg_{18}$ | 8.20 | 9.15 | 9.26 | 9.16 | 8.9 |
| $Arg_{19}$ | 10.0 | 8.56 | 8.71 | 8.31 | 7.99 |
| $Cys_{20}$ | 9.70 | 9.29 | 9.37 | 9.22 | 9.27 |
| R | | 1.34 | 1.06 | 1.01 | 1.14 |

Last row indicates the average distance (see Methods) between experimental (NMR) and theoretical (MD) values.

$\beta$-hairpin. The type I′ $\beta$-turn conformation derived from NMR data was generally observed during MD but replaced by either a type IV $\beta$-turn or a coil conformation of residue $Val_{13}$ ($\varphi_{13}$ fluctuated around $-83^{\circ}$ instead of its original value ($-141^{\circ}$). Despite the loss of the hydrogen bond and backbone dihedral transitions the overall structure of the fragment $Ile_{10}$-$Val_{13}$ remained in turn-like conformation. The torsion angle of $C^{\alpha}$ of the region $Ile_{10}$-$Val_{13}$ fluctuated in the region $[-60^{\circ}, 0^{\circ}]$ for the whole trajectory. The $Ile_{10}$:$C^{\alpha}$-$Val_{13}$:$C^{\alpha}$ distance escaped from the 0.7 nm cutoff which is generally acceptable for $\beta$-turns.

Figure 3 shows $C^{\alpha}$ atoms distance/dihedral contour plots of the $Arg_9$-$Ile_{10}$-$Arg_{11}$-$Gly_{12}$ and $Ile_{10}$-$Arg_{11}$-$Gly_{12}$-$Val_{13}$ peptide fragments of arenicin-2 in the four MD trajectories, while Table IV summarizes the existence of specific types $\beta$-turns in the four MD trajectories. The simultaneous existence of two consecutive $\beta$-turns that connect arenicin $\beta$-strands were supported by all MD trajectories, although one $\beta$-turn was not present for 100% of the frames. However, not all the trajectories showed the same preference. Type IV $\beta$-turn of the $Arg_9$-$Gly_{12}$ fragment was retained for 91.7% of the frames during M1 trajectory, but only 40%—during c14 trajectory. At the same time, $\beta$-turn of the fragment $Ile_{10}$-$Val_{13}$ was retained for only 29% of the frames in M1, while trajectories M3, 310K, and c14 retained the $\beta$-turn of the fragment $Ile_{10}$-$Val_{13}$ in almost 100% of the frames.

These discrepancies between NMR and MD structures are consistent with the distance found between $Ile_{10}$:$H^{N}$ and $Val_{13}$:$H^{N}$ protons. The corresponding input distance in the NMR-based calculations was 0.302 nm. The averaged distance during M1 trajectory was found to be 0.46 nm, while it remained $\sim$0.37 nm during M3, 310K, and c14 trajectories (see Supporting Information). This result underlines that M1 trajectory, while retaining the overall structure of arenicin-2, failed to reproduce correctly the local structure around $Ile_{10}$-$Val_{13}$ fragment.

## Hydrogen Bonds

Numerous hydrogen bonds appeared to stabilize the supersecondary structure of arenicin-2. Table V lists the hydrogen bond status of the main chain amide groups. There are six well-established hydrogen bond pairs between backbone donors and acceptors: $Val_4$:N-$Arg_{19}$:O, $Ala_6$:N-$Tyr1_{17}$:O, $Val_8$:N-$Val_{15}$:O, $Val_{15}$:N-$Val_8$:O, $Tyr_{17}$:N-$Ala_6$:O and $Arg_{19}$:N-$Val_4$:O. Four of these hydrogen bonds were found in more than 90% of the frames in all MD trajectories and contributed to the hairpin stability. Hydrogen bond between $Val_4$:N and $Arg_{19}$:O was found in trajectories M1 and M3 in $\sim$75% of the time. Raising the simulation temperature to 310 K resulted in decrease of this percentage to 54%. Surprisingly, applying a bigger cutoff of nonbonded interactions (c14 trajectory) totally diminished the existence of the $Val_4$:N-$Arg_{19}$:O hydrogen bond. $Tyr_{17}$:N-$Ala_6$:O hydrogen bond was not observed during M3 trajectory, while it was found in more than 95% in trajectories M1, 310K, and c14. The hydrogen bond $Val_{13}$:N-$Ile_{10}$:O that stabilized the type I′ $\beta$-turn of the fragment $Ile_{10}$-$Arg_{11}$-$Gly_{12}$-$Val_{13}$ in the NMR bundle of structures was poorly conserved during the MD trajectories, with percentage ranging from 0% (M1) to 45% (M3). The absence of this hydrogen bond interaction in the M1 trajectory is consistent the $\psi_{10}/\varphi_{11}$ dihedral angle transition observed during this MD trajectory. Moreover, the low percentages of occurrence are in agreement with the increased RMSF values of $C^{\alpha}$ atoms of this peptide's region (Figure 1). Thus, the higher backbone mobility resulted in loss of this specific interaction.

Relative instability of the central $\beta$-turn during the simulations might be attributed to its lower contribution to peptide conformational stability. Simulations of model peptides showed that the $\beta$-turn connecting the two antiparallel strands of the hairpin could be a relatively late event in the folding process.[39] In another study,[40] it was demonstrated that hydrophobic collapse of a model peptide proceeded to

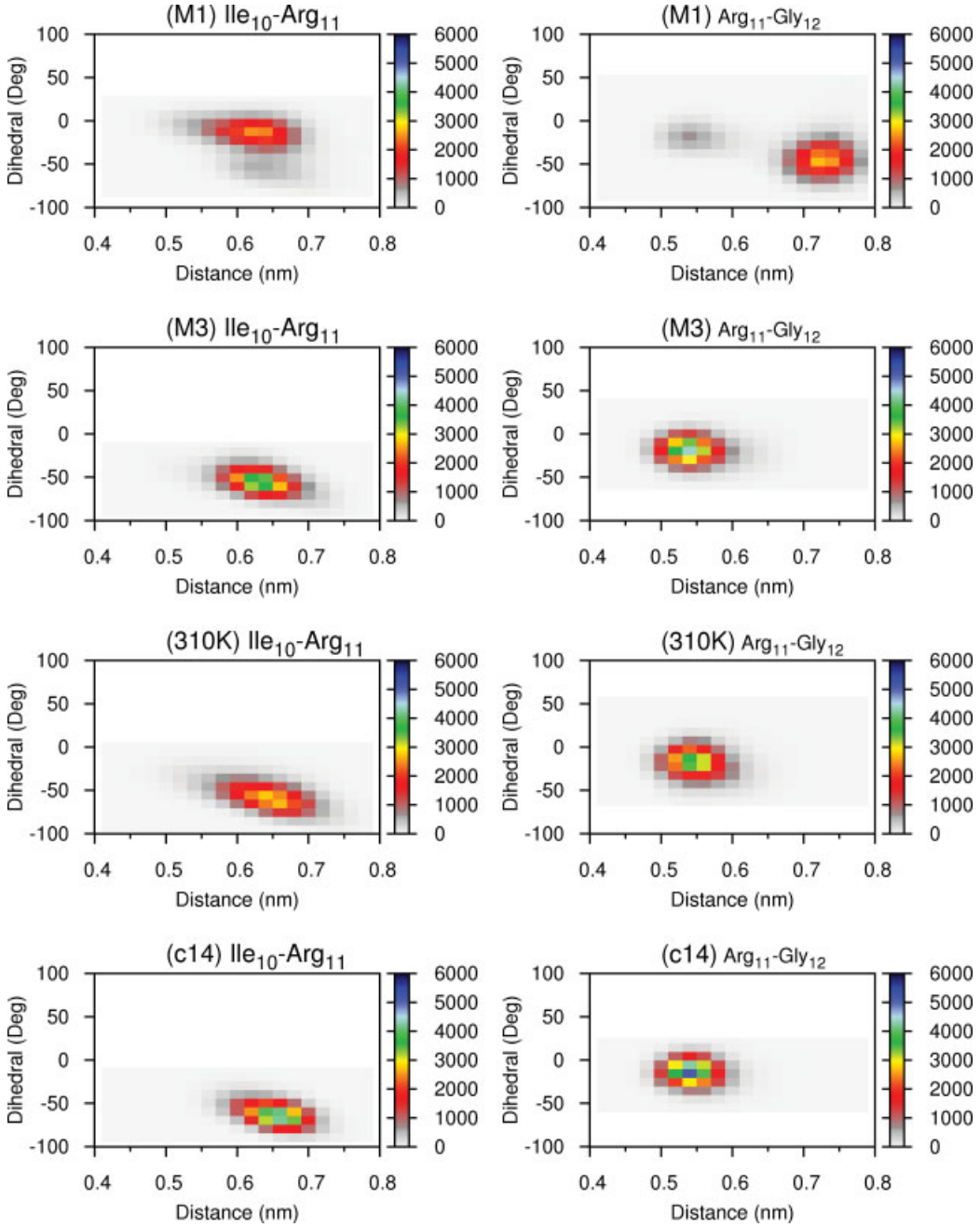


**FIGURE 3** Contour maps of distance and dihedral angle of the $Arg_9$-$Gly_{12}$ and $Ile_{10}$-$Val_{13}$ fragment. Distance C($i$)α-C($i$ + 3)α is plotted horizontically and dihedral C($i$)α-C($i$ + 1)α-C($i$)α-C($i$ + 2)α-C($i$ + 3)α is plotted vertically. Axis $z$ displays the number of frames found within 0.02 nm distance bin and 10° dihedral bin.

the canonical $\beta$-turn formation. Thus, our observation of low $\beta$-turn stability could be attributed to the time scale of simulation experiment: more time is needed to capture this folding process.[41] A hairpin nucleation at the turn is expected to be intrinsically rapid for a strong turn, as the process is driven by local forces at the turn site. For the hairpin with a weaker turn, the process must involve a collapse of hydrophobic side chains across the strands, the nucleation should be slower as solvent molecules must be displaced to allow sequestering of the hydrophobic residues.[42] For example, simulation of chignolin (the shortest stable $\beta$-hairpin in solution) indicated that the folding process did not follow the zipper mechanism but hydrophobic collapse proceeded the $\beta$-turn formation.[43]

**Table IV** **β-Turn Occurrence in the $Ile_{10}$-$Arg_{11}$ and $Arg_{11}$-$Gly_{12}$ Fragments During the Four MD Trajectories**

| | | % Occurrence | | | |
|---|---|---|---|---|---|
| Sequence | Type | M1 | M3 | 310K | c14 |
| $Ile_{10}$-$Arg_{11}$ | IV | 91.7 | 69.0 | 57.6 | 40.1 |
| $Arg_{11}$-$Gly_{12}$ | IV | 23.0 | 40.4 | 65.5 | 64.2 |
| | II′ | 5.3 | 58.6 | 33.0 | 35.4 |

## Overall Geometry of the β-Hairpin

According to previous NMR investigation of arenicin-2 in aqueous solution β-hairpin of the peptide is significantly kinked and twisted[5] (Figure 2). Simple geometric analysis (see Material and Method) revealed that in the NMR-derived set of structures the hairpin had the kink angle of 35° ± 4°, and right-handed twist of 213° ± 8° (per eight residues). To investigate the dynamical aspects of distortions in the β-hairpin structure, the present 50 ns MD trajectories were analyzed. The results (Figure 4) indicate that during the entire simulation the kink and twist angles remain approximately conserved. For the kink angle average values (and standard deviations) were found to be 36° (8°), 27° (7°), 30° (10°), and 34° (8°) for the M1, M3, 310K, and c14 trajectories, respectively. For the *twist* angle average values (and standard deviations) were found to be 189°(18°), 211°(15°), 199°(19°) and 211°(17°) for the M1, M3, 310K, and c14 trajectories, respectively. Overall, the results from MD trajectories were in good agreement with the NMR results, with c14 trajectory to be slightly better in reproducing the twist and kink average values. Figure 4 indicates that the increase of the kink angle (M1 trajectory) to the level of about 50° was observed at 10 ns and continued until 27 ns, then the kink value dropped below 40°. Interestingly, this temporary increase in the kink angle coincides with a temporary increase in the RMSD value computed with respect to the initial NMR coordinates of arenicin (Figure 1) and with disruption of some side-chain interactions. Comparison with RMSD values computed for different peptide regions indicates that the increase in the kink angle is not coupled with changes in conformation of β-turn, but rather involves small changes in conformation of N- and C-terminal strands of the peptides; the changes may be also involved in relative orientation of the two strands. Conversely, a slight decrease in the twist angle to the average level below 180° was observed within 7–20 ns interval of the simulation. This decrease does not stand out sharply against the background noise and possibly does not correlate with the increase in the kink value.

The observed twisting of the arenicin β-hairpin gives an overall right-handed twist of about 25° per residue. This value is in the range (0°–30°) reported for other β-structural proteins.[37,44] According to the recently updated large survey of protein structures,[45] the largest twist is observed for isolated two-stranded ribbons. In this respect, some other β-hairpin antimicrobials (e.g. gomesin[10] and protegrin-1[14]) also demonstrate a significant right-handed twist in solution.

## Side Chain Interactions

It is generally admitted that β-hairpins are stabilized not only by the hydrogen bond network but also via various types of other noncovalent interactions. The arenicin-2 β-hairpin structure, beyond backbone hydrogen bonds, was found to be stabilized by a plethora of side chain interactions of various types. Hydrophobic interactions, aromatic stacking, and cation/π-aromatic interactions were found to contribute to the stability of the arenicin-2 β-hairpin in aqueous solution. These nonbonded interactions proved to contribute to hairpin stability in several other cases.[46–48]

Side chains of $Val_8$, $Ile_{10}$, $Val_{15}$, and (to a lower degree) $Val_{13}$ formed a well conserved hydrophobic core. Figure 5 shows the time evolution of selected distances between side chains of $Val_8$, $Ile_{10}$, $Val_{13}$, and $Val_{15}$. These chains were found in close contact for more than 60% of the simulation time (∼100% in some cases, such as $Val_8$-$Val_{15}$). If we take into consideration the two hydrogen bonds between $Val_8$ and $Val_{15}$ then the significance of the two valine residues at positions 8 and 15 is easy to understand. Hydrophobic interactions between these residues remained strong during the whole trajectory and contributed to the stability of the β-hairpin structure acting as a supplementary power to the not so well conserved β-turn around the $Ile_{10}$-$Val_{13}$ fragment.

Nonbonded interactions between planar groups of amino acids are of significant importance in protein structure stabilization. Various types of such interactions were identified.[49] We observed cation/π-aromatic stacking between arginine

**Table V** **Hydrogen Bonds of Arenicin's Backbone Atoms**

| | | % Occurrence | | | |
|---|---|---|---|---|---|
| Donor | Acceptor | M1 | M3 | 310K | c14 |
| $Val_4$ | $Arg_{19}$ | 78.6 | 74.3 | 53.6 | |
| $Ala_6$ | $Tyr_{17}$ | 96.4 | 94.7 | 94.8 | 97.8 |
| $Val_8$ | $Val_{15}$ | 96.6 | 94.1 | 95.6 | 96.0 |
| $Ile_{10}$ | $Val_{13}$ | 14.0 | 88.8 | 86.6 | 92.7 |
| $Val_{13}$ | $Ile_{10}$ | | 45.2 | 35.6 | 32.4 |
| $Val_{15}$ | $Val_8$ | 97.2 | 94.8 | 95.7 | 95.8 |
| $Tyr_{17}$ | $Ala_6$ | 96.2 | | 95.1 | 94.4 |
| $Arg_{19}$ | $Val_4$ | 96.8 | 98.3 | 94.5 | 94.6 |

Percentage of occurrence is given for the four MD trajectories.

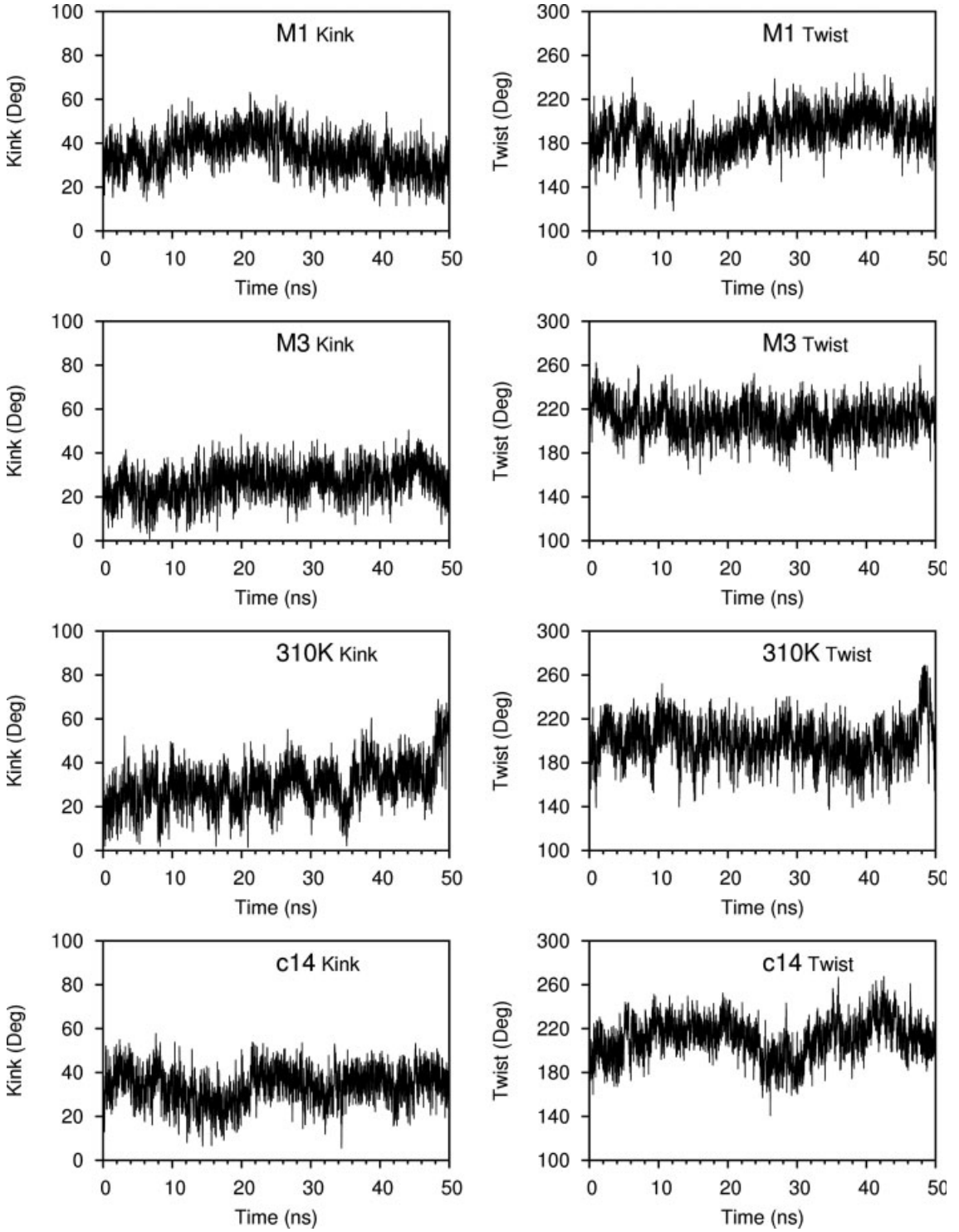


**FIGURE 4** Time series of kink and twist angles of arenicin's $\beta$-hairpin.

and tyrosine or/and tryptophan aromatic side chains. The strongest interactions were found between $Tyr_5$ and $Arg_{16}$ side chains, although other combinations were found as well (Supporting Information). The guanidinium and aryl groups were found in almost parallel alignment and quite close to each other. Figure 6 shows the distance between the two planar groups remained less than 0.6 nm almost all the time. Simultaneously, they appeared in parallel configuration indi-

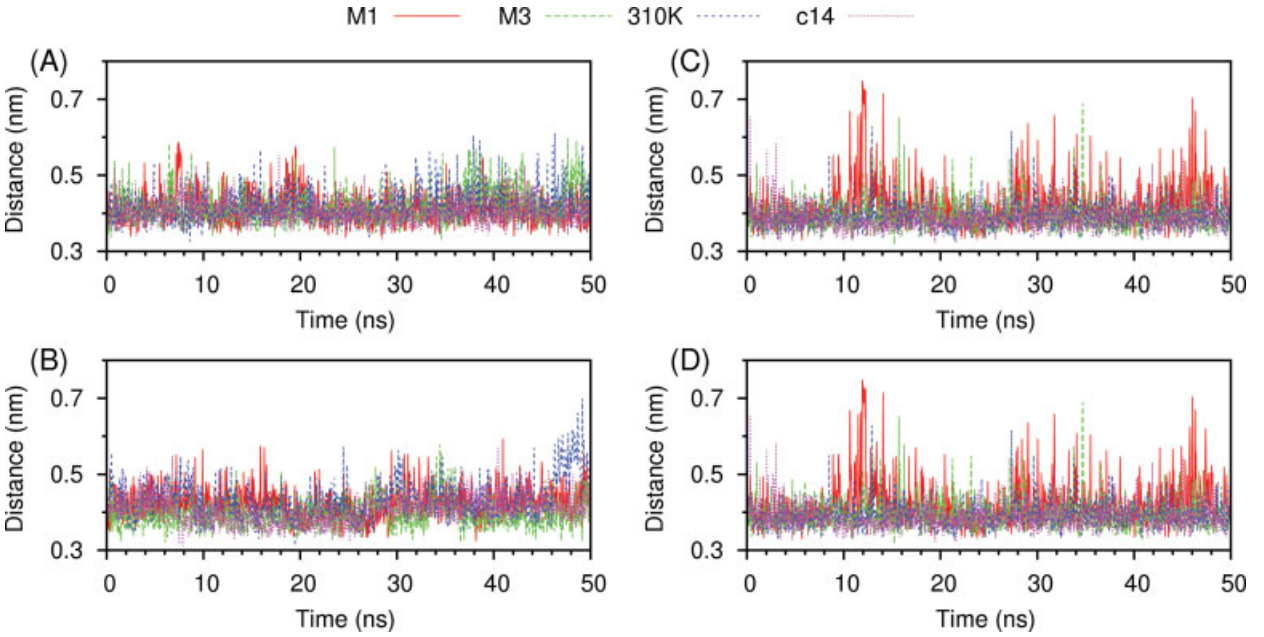


**FIGURE 5** Time evolution of distances between aliphatic side chains of (A) $Val_8$-$Ile_{10}$, (B) $Val_8$-$Val_{15}$, (C) $Ile_{10}$-$Val_{15}$, and (D) $Val_{13}$-$Val_{15}$ during the four MD trajectories. The shortest distance among carbon atoms of the corresponding side chains is plotted.

cating their preference for side chain stacking. These two residues lay in the center of the two strands and their backbone atoms do not participate in hydrogen bonding. The $\chi^1$ dihedral angle of $Tyr_5$ averaged $-41^\circ$ ($-34^\circ$ according to NMR data) while $\chi^1$ dihedral angle of $Arg_{16}$ averaged $-30^\circ$ ($-50^\circ$ according to NMR data). This smooth dihedral angles shift

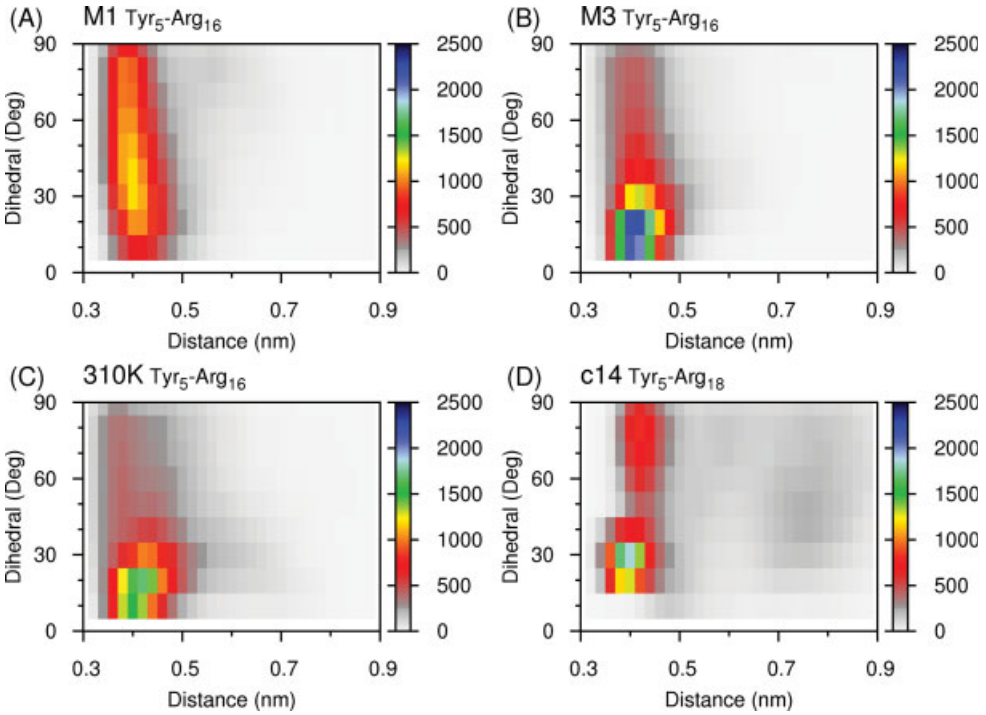


**FIGURE 6** Distance and dihedral contour plots between $Tyr_5$/$Arg_{16}$ side chain planar groups. Axis *z* (contours) shows number of frames found within 0.02 nm distance bin and 10° dihedral bin. (A) M1 trajectory, (B) M3 trajectory, (C) 310K trajectory, and (D) c14 trajectory.

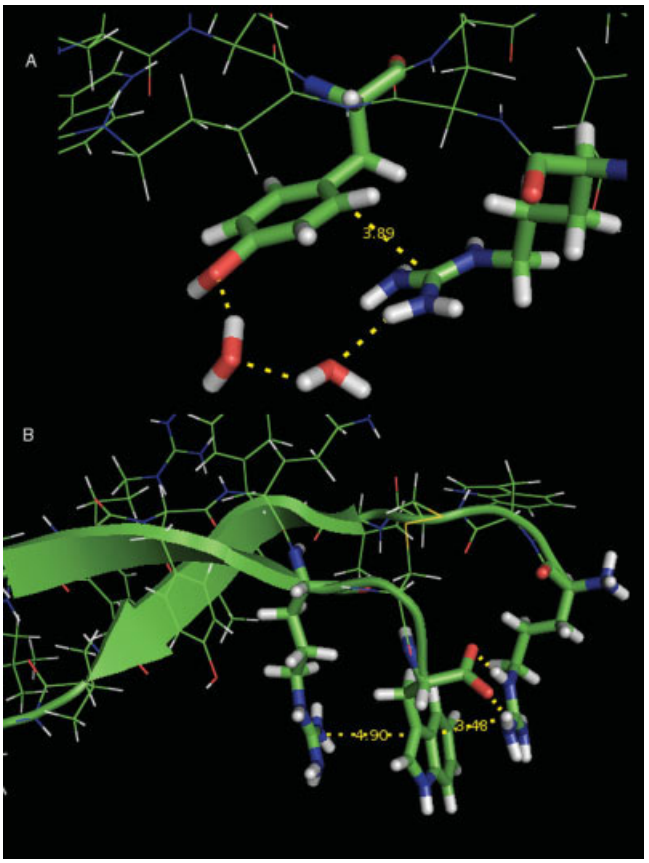


**FIGURE 7** Weak interactions found in MD trajectories. (A) Network of hydrogen bonds between Tyr5/Arg16 side chains. (B) Parallel stacking of $Arg_{19}/Trp_{21}/Arg_1$ side chains facilitated by $Trp_{21}$-$Arg_1$ salt bridge.

allowed a better side chain alignment and favored their parallel stacking. Both side chains of $Tyr_5$ and $Arg_{16}$ were found to be hydrogen bonded to water molecules. Interestingly, water donor to tyrosine $O^{\eta}$ atom was hydrogen bonded to water that accepted a hydrogen bond from the guanidinium group. Figure 7 illustrates this interaction network being quite stable during MD trajectory. To a lower extend, interactions between $Arg_{18}/Tyr_5$ were also recorded.

N-terminal $Arg_1$, $Arg_{19}$, and C-terminal $Trp_{21}$ were also found to be involved in cation/$\pi$-aromatic interactions. For example in the M1 trajectory during the first 10 ns of the simulation only the $Arg_1/Trp_{21}$ interaction was observed. The two side chains were then separated until ~27 ns. At this point and until 40 ns a simultaneous proximity of the $Arg_1$ and $Arg_{19}$ guanidinium groups to both sides of the tryptophan side chain was observed. This double stacking was facilitated by the salt bridge formed between the $Arg_1$ side chain and the $Trp_{21}$ C-terminal carboxyl group. Because of the above-mentioned strong electrostatic interactions between the $Arg_1$ and $Trp_{21}$ polar groups, the two corresponding side chains were found in quite close proximity until ~40 ns when the interactions were broken down and reappeared only sporadically by the end of simulation. On the contrary, $Arg_{19}/Trp_{21}$ side chain stacking remained relatively stable until the end of the 50 ns simulation time.

T-shaped interactions between arginine and aromatic residues side chains were also observed. In most cases, the same pair of side chains was found to be partly in parallel and partly in vertical alignment. For example, as it can be seen from Table VI, $Tyr_5$ and $Arg_{16}$ side chains were found in T-shaped interaction in all MD trajectories for percentage ranging from 28% to 55%.

It is thus evident that both parallel (stacked) and vertical (T-shaped) alignment of planar groups was in presence. The dihedral angle ($\alpha$) between side chain planar groups was measured and classified in three state model: parallel ($\alpha < 30^\circ$), vertical ($\alpha \geq 60^\circ$) and others ($\alpha \geq 30^\circ$, $\alpha < 60^\circ$). Frequencies of transition (from any state to any other) were measured for the $Tyr_5/Arg_{16}$ side chain interaction; this pair appeared to exhibit strongest stacking interaction among all other possible pairs (Figure 6). Arrangements (parallel/vertical/other) between planar side chains changed quite frequently during MD. Calculated number of transitions between different arrangements (parallel/vertical/other, for details see Methods) was found to be 17,511, 23,978, and 16,387 in M1, M3, and 310K MD trajectories, respectively. This means that side chain alignment changed state every (approximately) 2–3 ps. The speed of this conformational change is untraceable by conventional experimental methods and atomistic MD simulations provide a very good framework for studying such phenomena.

We did not observe any direct hydrogen bonding by side chains. Some hydrogen bond interactions between arginine and tyrosine side chains could be expected, but the overall structure of the peptide-favored $\pi$ stacking, or T-shaped

**Table VI Percentage of Occurrence of Parallel (Stacking) or Vertical (T-Shaped) Alignment of Side Chains of Arg/Tyr/Trp Residues**

| | M1 | | M3 | | 310K | | c14 | |
|---|---|---|---|---|---|---|---|---|
| Pair | Par. | Ver. | Par. | Ver. | Par. | Ver. | Par. | Ver. |
| $Arg_1 - Trp_2$ | | | | | | | 52.7 | |
| $Arg_1 - Trp_{19}$ | 25.7 | | | | | | | |
| $Arg_1 - Trp_{21}$ | 24.7 | | 32.2 | 58.2 | | | | |
| $Trp_2 - Arg_{18}$ | | | | | | | 33.0 | |
| $Tyr_5 - Arg_{16}$ | 28.5 | 32.6 | 54.9 | 37.8 | 48.6 | 27.1 | | 43.3 |
| $Tyr_5 - Arg_{18}$ | | | | | | | 24.2 | 42.8 |
| $Arg_{19} - Trp_{21}$ | | | 31.2 | 32.0 | | | | |

See Methods for geometrical criteria applied.

interactions of these side chains as mentioned above. However, side chain to main chain hydrogen bonds took place to some extent. For example, $Arg_9$:$N^{\eta 11}$ and $Arg_9$:$N^{\varepsilon}$ was found to be hydrogen bonded with $Gly_{12}$:O in 42% and 18% of the time, respectively. $Arg_{11}$:O was hydrogen bonded with guanidium atoms of $Arg_9$ for 12% of the simulation time.

Another interesting interaction took place between the side chains of $Ala_6$ and $Tyr_{17}$. These side chains formed a CH. . .$\pi$ aromatic bond, one of the weakest in protein interactions.[50] However, we found it to be quite stable during all MD trajectories. The distance between $Ala_6$:$C^{\beta}$ and the center of mass of $Tyr_{17}$ aromatic ring fluctuated with mean value of 0.49 nm (averaged over all the four trajectories). This interaction remained stable despite other conformational transitions that occurred during MD trajectory. Side chain $\chi^1$ angle of $Tyr_{17}$ residue was found to be 74.9° (7.7°) in M1, 73.5° (8.0°) in M3, 73.2° (15.5°) in 310K and 74.7° (7.9°) in c14 trajectories respectively, in agreement with the NMR data: 66.4° (5.4°). Taking into account that these two residues interacted with each other with two backbone hydrogen bonds, displaying only limited conformational mobility, the CH. . .$\pi$ aromatic bond acted as an extra lock of the conformation of the two residues in the middle of the $\beta$-sheet.

## Water Structure Around Arenicin-2

As expected from their polar nature, arginine residues appeared highly hydrated. For $Arg_9$ and $Arg_{11}$ residues, each hydrogen atom of guanidinium side chain group was found to be hydrogen bonded with water for ~47% of the time (M1 trajectory). $Arg_{16}$, $Arg_{18}$, and $Arg_{19}$ residues showed an increased hydration, and each of their polar side chain hydrogen atoms was hydrated for ~77% of the time. Bearing in mind that each guanidinium group has five hydrogen atoms, the previous analysis means that the arginine side chain hold approximately from 2.5 to 4 water molecules in the first solvation shell.

Side chains of tyrosine residues were also found to form hydrogen bonds with water although the hydroxyl group acted mainly as a donor. Hydroxyl $H^{\eta}$ atom was found in a hydrogen bond state with water oxygen in 81% ($Tyr_{17}$), 79% ($Tyr_5$), or 69% ($Tyr_7$) of the total trajectory. The tryphophan side chain $H^{\varepsilon 1}$ atom was found to be hydrogen bonded with water in 71% and 64% for $Trp_2$ and $Trp_{21}$, respectively.

## Comparison of NOE Distances and $^3J$ ($H^N$-$H^{\alpha}$) Coupling Constants

Table III lists the experimental and MD-calculated $^3J$($H^N$-$H^{\alpha}$) coupling constants. With the exception of the $Arg_{11}$ $^3J$, that corresponds to the $\varphi_{11}$ backbone dihedral angle, all trajectories produced results being in fairly good agreement with the experiment. Average square distance values ($R_{3J}$) for $^3J$ ranged from 1.01 Hz (310K MD trajectory) to 1.34 Hz (M1 MD trajectory). The discrepancy of the M1 trajectory, concerning the $Arg_{11}$, is in agreement with the transition of $\varphi_{11}$ dihedral angle discussed earlier. However, in all other cases, the agreement of the NMR (restrained dynamics in torsion space) and current MD simulation (unrestrained dynamic in Cartesian space) is very good.

Average distances from the four MD trajectories that correspond to $H^N$, $H^{\alpha}$, and $H^{\beta}$ atoms were calculated on the $<r^{-1/6}>^{1/6}$ basis (see Methods). Detailed results are provided in the supporting information. It was found that all four MD trajectories gave results in great consistency with the input NOE restraints, used in NMR based structure calculation of arenicin-2. Majority atom pairs showed MD-averaged distances below the NMR based upper limit. The largest discrepancies between calculated averaged distances and experimental NOE-based restraints were found in the region of $\beta$-turn. This situation was generally expected, as this region of the hairpin is probably subjected to elevated conformational dynamics (see above).

Both $^3J$ and NOE calculations, based on MD data, provide evidence for the reliability of the MD results. Such cross-validations are very important for the interpretation of modeling-derived results.[19,51,52]

# CONCLUSIONS

Four MD trajectories of the antimicrobial peptide arenicin-2 in explicit water were produced under various conditions in order to get a clear view of the peptide structure. The structures resulted from computer simulation were found in fairly good agreement with experimental (NMR) data, concerning $^3J$ coupling constants and NOE-derived proton distances. Moreover, MD trajectories produced the structures close to the NMR-derived backbone conformation of arenicin-2, even at elevated temperature. Only in one (M1) trajectory two backbone angles ($\psi_{10}/\varphi_{11}$) escaped significantly from the initial values. The simulated structures of arenicin-2 offered an opportunity to carefully analyze the nonbonded interactions of the side chains that stabilize the $\beta$-hairpin structure, something that it is generally hardly achieved by solution NMR methods, mainly due to high mobility of side chains in aqueous environment. From this point of view, the current study complements the NMR-based structural information about the arenicin solution conformation. Robustness of the results (checked by four independent MD trajectories) ensures the quality of the proposed extent of nonbonded side chain interactions. Thus, aromatic/$\pi$ (both stacked and

T-shaped), aromatic/C-H and hydrophobic interactions between side chain groups contributed to the stability of the arenicin $\beta$-hairpin structure.

Presently, it is generally assumed that a cellular membrane is the main target of the arenicin antimicrobial action. According to the recent models, the peptide binds to the surface of the bacterial membrane and disrupts the membrane integrity via formation of ion-conducting defects or pores.[53,54] The NMR structural data obtained in DPC micelles environment indicate that these ion-conducting pores can be composed from the $\beta$-structural oligomers of the peptide.[53] It was proposed that side-by-side parallel dimer of the $\beta$-hairpins (CN↑↑NC type of association) was the main building block of the arenicin pore.

Knowledge of a membrane-active peptide structure and dynamics in aqueous solution is of importance for full description of its mode of action. Indeed, changes in the peptide free energy (including enthalpy and entropy contributions) on membrane binding and insertion determine the effectiveness of these processes. The present results on molecular dynamic simulation point to structural and dynamic determinants that underlie the arenicin membrane activity and selectivity. (1) The peptide $\beta$-turn and two associated backbone hydrogen bonds were found to be disrupted in water solution. This distortion from ideal hairpin conformation is possibly stabilized by side-chain interactions in the cluster of hydrophobic residues ($Val_8$, $Ile_{10}$, $Val_{13}$, and $Val_{15}$). Now we can speculate that upon association with the membrane these hydrophobic interactions will be substituted by side-chain/lipid interactions and the classical $\beta$-hairpin hydrogen bonding will be restored. This should increase the enthalpy contribution to the membrane affinity. (2) The weak cation/$\pi$-aromatic side-chain interactions, observed in the simulation, can also be influenced by a contact with the membrane surface. In case of partially anionic bacterial membrane these interactions can be substituted by more energetically favorable hydrophobic interactions of aromatic residues with lipid tails and by electrostatic interactions of Arg residues with charged lipid head groups. That must significantly contribute to the membrane affinity. Conversely, in case of zwitterionic eukaryotic membranes the electrostatic interactions will be less effective, and such a transformation of interactions might be even energetically costly. (3) The absence of significant intramolecular motions in the distorted arenicin hairpin in water solution should diminish the entropic penalty of the peptide immobilization at the lipid interface.

The evidence supporting the above mentioned ideas can be gained from previous NMR and CD spectroscopic investigations of the peptide in the detergent micelles.[6,53] First of all, the CD spectra of arenicin-2 experience significant changes upon detergent addition and have more canonical $\beta$-structural appearance in micelle bound form (DPC and SDS).[6] At the same time, the NMR data indicate the preservation of the $\beta$-hairpin secondary structure upon DPC micelle incorporation[53] pointing to some other rearrangements in the peptide structure (e.g. formation of more classical $\beta$-turn or untwisting of the $\beta$-sheet) as the major cause of CD spectra changes. Secondly, the observed strong binding of the peptide to the partially anionic vesicles (POPE/POPG 7:3) and the absence of detectable peptide binding to the zwitterionic vesicles (POPC)[6] prove an important role of electrostatic interactions in the arenicin membrane activity.

The results of the current molecular dynamic simulation also strongly support the presence of significant right-handed twist and kink in the $\beta$-hairpin of arenicin-2 in aqueous environment. The examination of the arenicin-2 spatial structure (Figure 2) allows us to propose that side-chain interactions on the $\beta$-hairpin ends ($Val_8$, $Ile_{10}$, $Val_{13}$, $Val_{15}$ on one side and $Arg_1$, $Arg_{19}$, $Trp_{21}$ on the other) are the main driving force for these distortions. In this case the overall geometry of the arenicin hairpin can also experience significant changes upon contact with hydrophobic region of cellular membrane or anisotropic membrane mimetic (e.g. detergent micelle). At present not enough experimental or theoretical data are available to describe these changes. However, assuming that the $\beta$-structural pore model of arenicin action is correct; we can compare the observed $\beta$-hairpin twist to the twists in the transmembrane $\beta$-barrel proteins. The published survey of $\beta$-barrel proteins indicates that they have average twist angles in the range of $7^\circ$–$18^\circ$ per residue.[44] Interestingly, the largest twist was observed for the shorter proteins having the $\beta$-strand length similar to that of arenicin (8–10 residues). If we compare the above data with an average arenicin twist ($25^\circ$ per residue) we can come to a conclusion that the peptide should experience some untwisting upon formation of a $\beta$-structural pore.

In summary, we can conclude that the current results represent a step towards understanding the mechanism of the arenicin membrane-mediated antibiotic action. However, molecular dynamic investigations of the peptide in lipid environment are needed for the further progress in this field.

Authors A.S. and I.G.T. wish to thank the Research Center of Scientific Simulations of University of Ioannina for providing the computational facilities for NAMD parallel execution.

## REFERENCES

1. Boman, H. G. Annu Rev Immunol 1995, 13, 61–92.
2. Epand, R. M.; Vogel, H. J. Biochim Biophys Acta 1999, 1462, 11–28.

3. Boman, H. G. J Intern Med 2003, 254, 197–215.
4. Zikou, S.; Koukkou, A. I.; Mastora, P.; Sakarellos-Daitsiotis, M.; Sakarellos, C.; Drainas, C.; Panou-Pomonis, E. J Pept Sci 2007, 13, 481–486.
5. Ovchinnikova, T. V.; Aleshina, G. M.; Balandin, S. V.; Krasnosdembskaya, A. D.; Markelov, M. L.; Frolova, E. I.; Leonova, Y. F.; Tagaev, A. A.; Krasnodembsky, E. G.; Kokryakov, V. N. FEBS Lett 2004, 577, 209–214.
6. Ovchinnikova, T. V.; Shenkarev, Z. O.; Nadezhdin, K. D.; Balandin, S. V.; Zhmak, M. N.; Kudelina, I. A.; Finkina, E. I.; Kokryakov, V. N.; Arseniev, A. S. Biochem Biophys Res Commun 2007, 360, 156–162.
7. Mandard, N.; Sodano, P.; Labbe, H.; Bonmatin, J. M.; Bulet, P.; Hetru, C.; Ptak, M.; Vovelle, F. Eur J Biochem 1998, 256, 404–410.
8. Hwang, P. M.; Zhou, N.; Shan, X.; Arrowsmith, C. H.; Vogel, H. J. Biochemistry 1998, 37, 4288–4298.
9. Trabi, M.; Schirra, H. J.; Craik, D. J. Biochemistry 2001, 40, 4211–4221.
10. Mandard, N.; Bulet, P.; Caille, A.; Daffre, S.; Vovelle, F. Eur J Biochem 2002, 269, 1190–1198.
11. Laederach, A.; Andreotti, A. H.; Fulton, D. B. Biochemistry 2002, 41, 12359–12368.
12. Lauth, X.; Babon, J. J.; Stannard, J. A.; Singh, S.; Nizet, V.; Carlberg, J. M.; Ostland, V. E.; Pennington, M. W.; Norton, R. S.; Westerman, M. E. J Biol Chem 2005, 280, 9272–9282.
13. Mandard, N.; Sy, D.; Maufrais, C.; Bonmatin, J. M.; Bulet, P.; Hetru, C.; Vovelle, F. J Biomol Struct Dyn 1999, 17, 367–380.
14. Fahrner, R. L.; Dieckmann, T.; Harwig, S. S.; Lehrer, R. I.; Eisenberg, D.; Feigon, J. Chem Biol 1996, 3, 543–550.
15. Mani, R.; Tang, M.; Wu, X.; Buffy, J. J.; Waring, A. J.; Sherman, M. A.; Hong, M. Biochemistry 2006, 45, 8341–8349.
16. Gupta, A.; Van Vlijmen, H. W.; Singh, J. Protein Sci 2004, 13, 2045–2058.
17. Stavrakoudis, A.; Tsikaris, V. J Pept Sci 2008, 14, 1259–1270.
18. Karplus, M.; McCammon, J. A. Nat Struct Biol 2002, 9, 646–652.
19. Zagrovic, B.; van Gunsteren, W. F. Proteins 2006, 63, 210–218.
20. Mehrnejad, F.; Naderi-Manesh, H.; Ranjbar, B. Proteins 2007, 67, 931–940.
21. Junkes, C.; Wessolowski, A.; Farnaud, S.; Evans, R. W.; Good, L.; Bienert, M.; Dathe, M. J Pept Sci 2007, 14, 535–543.
22. Gallivan, J. P.; Dougherty, D. A. Proc Natl Acad Sci USA 1999, 96, 9459–9464.
23. Meyer, E. A.; Castellano, R. K.; Diederich, F. Agnew Chem Int Ed Engl 2003, 42, 1211–1248.
24. Humphrey, W.; Dalke, A.; Schulten, K. J Mol Graph 1996, 14, 33–38.
25. Jorgensen, W. L.; Chandrasekhar, J.; Madura, J. D.; Impey, R. W.; Klein, M. L. J Chem Phys 1983, 79, 926–935.
26. Weber, W.; Hünenberger, P. H.; McCammon, J. A. J Phys Chem B 2000, 104, 3668–3675.
27. MacKerell, A. D.; Bashford, D.; Bellott, M.; Dunbrack, R. L.; Evanseck, J. D.; Field, M. J.; Fischer, S.; Gao, J.; Guo, H.; Ha, S.; Joseph-McCarthy, D.; Kuchnir, L.; Kuczera, K.; Lau, F. T. K.; Mattos, C.; Michnick, S.; Ngo, T.; Nguyen, D. T.; Prodhom, B.; Reiher, W. E.; Roux, B.; Schlenkrich, M.; Smith, J. C.; Stote, R.; Straub, J.; Watanabe, M.; Wiorkiewicz-Kuczera, J.; Yin, D.; Karplus, M. J Phys Chem B 1998, 102, 3586–3616.
28. Phillips, J. C.; Braun, R.; Wang, W.; Gumbart, J.; Tajkhorshid, E.; Villa, E.; Chipot, C.; Skeel, R. D.; Kale, L.; Schulten, K. J Comput Chem 2005, 26, 1781–1802.
29. Darden, T.; York, D.; Pedersen, L. J Chem Phys 1993, 98, 10089–10092.
30. Ryckaert, J. P.; Ciccotti, G.; Berendsen, H. J. C. J Comput Phys 1977, 23, 327–341.
31. Feller, S. E.; Zhang, Y. H.; Pastor, R. W.; Brooks, B. R. J Chem Phys 1995, 103, 4613–4621.
32. Glykos, N. M. J Comput Chem 2006, 27, 1765–1768.
33. Frishman, D.; Argos, P. Proteins 1995, 23, 566–579.
34. Delano, W. The PYMOL Molecular Graphics System; Delano Scientific: San Carlos, CA, 2002.
35. Wang, A. C.; Bax, A. J Am Chem Soc 1996, 118, 2483–2494.
36. Levitt, M.; Perutz, M. F. J Mol Biol 1998, 201, 751–754.
37. Richardson, J. S. Adv Prot Chem 1981, 34, 167–339.
38. Yonetani, Y. J Chem Phys 2006, 124, art. no. 204501.
39. Santiveri, C. M.; Jimenez, M. A.; Rico, M.; Van Gunsteren, W. F.; Daura, X. J Pept Sci 2004, 10, 546–565.
40. Yoda, T.; Sugita, Y.; Okamoto, Y. Proteins 2007, 66, 846–859.
41. Duan, Y.; Kollman, P. A. Science 1998, 282, 740–744.
42. Kuo, N. N.; Huang, J. J.; Miksovska, J.; Chen, R. P.; Larsen, R. W.; Chan, S. I. J Am Chem Soc 2005, 127, 16945–16954.
43. Suenaga, A.; Narumi, T.; Futatsugi, N.; Yanai, R.; Ohno, Y.; Okimoto, N.; Taiji, M. Chem Asian J 2007, 2, 591–598.
44. Pali, T.; Marsh, D. Biophys J 2001, 80, 2789–2797.
45. Richardson, J. S. Available at: http://sunabiochemdukeedu/teaching/anatax/indexhtml.
46. Espinosa, J. F.; Syud, F. A.; Gellman, S. H. Protein Sci 2002, 11, 1492–1505.
47. Syud, F. A.; Stanger, H. E.; Gellman, S. H. J Am Chem Soc 2001, 123, 8667–8677.
48. Wang, H.; Sung, S. S. Biopolymers 1999, 50, 763–776.
49. Chakrabarti, P.; Bhattacharyya, R. Prog Biophys Mol Biol 2007, 95, 83–137.
50. Bazzicalupi, C.; Dapporto, P. Structural Chemistry 2004, 15, 259–268.
51. Trzesniak, D.; Glattli, A.; Jaun, B.; van Gunsteren, W. F. J Am Chem Soc 2005, 127, 14320–14329.
52. van Gunsteren, W. F.; Dolenc, J.; Mark, A. E. Curr Opin Struct Biol 2008, 18, 149–153.
53. Ovchinnikova, T. V.; Shenkarev, Z. O.; Balandin, S. V.; Nadezhdin, K. D.; Paramonov, A. S.; Kokryakov, V. N.; Arseniev, A. S. Biopolymers 2008, 89, 455–464.
54. Andra, J.; Jakovkin, I.; Grotzinger, J.; Hecht, O.; Krasnosdembskaya, A. D.; Goldmann, T.; Gutsmann, T.; Leippe, M. Biochem J 2008, 410, 113–122.

# Supplementary material for: "Molecular dynamics simulation of antimicrobial peptide arenicin-2: β-hairpin stabilization by noncovalent interactions"

Athanassios Stavrakoudis,[a] Ioannis G. Tsoulos,[b] Zakhar O. Shenkarev,[c] Tatiana V. Ovchinnikova[c]

[a]Department of Economics, University of Ioannina, GR-45110, Ioannina, Greece
[b]Department of Computer Science, University of Ioannina, GR-45110, Ioannina, Greece
[c]Shemyakin and Ovchinnikov Institute of Bioorganic Chemistry, Russian Academy of Sciences, Miklukho-Maklaya str., 16/10, 117997 Moscow, Russia

Table 1: Experimental upper limit restraints (NOE) used for NMR calculation (see ref. 6) and averaged values from the four MD trajectories of $H^N$,$H^\alpha$,$H^\beta$ protons of arenicin-2.

| **Atom Pair** | **NMR UPL** | **Average Distance** | | | |
|---|---|---|---|---|---|
| | | **M1** | **M3** | **310K** | **c14** |
| $Arg_1$:$H^\alpha$–$Trp_2$:$H^N$ | 0.265 | 0.251 | 0.245 | 0.242 | 0.315 |
| $Trp_2$:$H^\alpha$–$Cys_3$:$H^N$ | 0.240 | 0.240 | 0.242 | 0.237 | 0.237 |
| $Trp_2$:$H^{\beta 3}$–$Cys_3$:$H^N$ | 0.430 | 0.242 | 0.260 | 0.256 | 0.331 |
| $Trp_2$:$H^N$–$Trp_{21}$:$H^N$ | 0.318 | 0.458 | 0.523 | 0.610 | 0.630 |
| $Cys_3$:$H^\alpha$–$Val_4$:$H^N$ | 0.240 | 0.223 | 0.226 | 0.227 | 0.237 |
| $Cys_3$:$H^{\beta 3}$–$Val_4$:$H^N$ | 0.331 | 0.394 | 0.384 | 0.378 | 0.360 |
| $Cys_3$:$H^\alpha$–$Cys_{20}$:$H^\alpha$ | 0.284 | 0.221 | 0.237 | 0.247 | 0.293 |
| $Cys_3$:$H^\alpha$–$Trp_{21}$:$H^N$ | 0.387 | 0.371 | 0.348 | 0.472 | 0.683 |
| $Val_4$:$H^\alpha$–$Tyr_5$:$H^N$ | 0.241 | 0.247 | 0.244 | 0.245 | 0.242 |
| $Val_4$:$H^\beta$–$Tyr_5$:$H^N$ | 0.282 | 0.229 | 0.231 | 0.229 | 0.234 |
| $Val_4$:$H^N$–$Arg_{19}$:$H^N$ | 0.290 | 0.331 | 0.338 | 0.352 | 0.389 |
| $Val_4$:$H^N$–$Cys_{20}$:$H^\alpha$ | 0.391 | 0.353 | 0.353 | 0.365 | 0.384 |
| $Tyr_5$:$H^\alpha$–$Ala_6$:$H^N$ | 0.240 | 0.220 | 0.220 | 0.219 | 0.218 |
| $Tyr_5$:$H^{\beta 3}$–$Ala_6$:$H^N$ | 0.346 | 0.411 | 0.409 | 0.411 | 0.410 |
| $Ala_6$:$H^\alpha$–$Tyr_7$:$H^N$ | 0.240 | 0.246 | 0.245 | 0.243 | 0.247 |
| $Ala_6$:$H^N$–$Tyr_{17}$:$H^N$ | 0.304 | 0.294 | 0.291 | 0.294 | 0.289 |
| $Tyr_7$:$H^\alpha$–$Val_8$:$H^N$ | 0.240 | 0.222 | 0.222 | 0.220 | 0.223 |
| $Tyr_7$:$H^\alpha$–$Arg_{16}$:$H^\alpha$ | 0.361 | 0.246 | 0.234 | 0.239 | 0.239 |
| $Val_8$:$H^N$–$Val_{15}$:$H^\beta$ | 0.412 | 0.369 | 0.467 | 0.377 | 0.381 |
| $Val_8$:$H^N$–$Val_{15}$:$H^N$ | 0.288 | 0.296 | 0.311 | 0.305 | 0.306 |
| $Arg_9$:$H^\alpha$–$Ile_{10}$:$H^N$ | 0.240 | 0.220 | 0.216 | 0.218 | 0.219 |
| $Arg_9$:$H^\alpha$–$Val_{15}$:$H^N$ | 0.359 | 0.327 | 0.319 | 0.331 | 0.331 |
| $Ile_{10}$:$H^\alpha$–$Arg_{11}$:$H^N$ | 0.240 | 0.287 | 0.217 | 0.217 | 0.219 |
| $Ile_{10}$:$H^N$–$Val_{13}$:$H^\beta$ | 0.560 | 0.547 | 0.400 | 0.426 | 0.430 |
| $Ile_{10}$:$H^N$–$Val_{13}$:$H^N$ | 0.302 | 0.455 | 0.366 | 0.369 | 0.385 |
| $Ile_{10}$:$H^N$–$Leu_{14}$:$H^\alpha$ | 0.401 | 0.408 | 0.346 | 0.347 | 0.341 |
| $Arg_{11}$:$H^\alpha$–$Gly_{12}$:$H^N$ | 0.287 | 0.354 | 0.344 | 0.343 | 0.349 |
| $Arg_{11}$:$H^N$–$Gly_{12}$:$H^N$ | 0.322 | 0.247 | 0.405 | 0.395 | 0.409 |

| Atom Pair | NMR UPL | Average Distance | | | |
|---|---|---|---|---|---|
| | | **M1** | **M3** | **310K** | **c14** |
| $Gly_{12}$:$H^N$–$Val_{13}$:$H^N$ | 0.308 | 0.231 | 0.216 | 0.215 | 0.219 |
| $Val_{13}$:$H^\alpha$–$Leu_{14}$:$H^N$ | 0.240 | 0.235 | 0.219 | 0.222 | 0.221 |
| $Leu_{14}$:$H^\alpha$–$Val_{15}$:$H^N$ | 0.240 | 0.218 | 0.220 | 0.218 | 0.219 |
| $Leu_{14}$:$H^N$–$Val_{15}$:$H^\beta$ | 0.314 | 0.667 | 0.682 | 0.625 | 0.651 |
| $Val_{15}$:$H^\alpha$–$Arg_{16}$:$H^N$ | 0.240 | 0.223 | 0.235 | 0.224 | 0.226 |
| $Val_{15}$:$H^\beta$–$Arg_{16}$:$H^N$ | 0.370 | 0.310 | 0.243 | 0.315 | 0.273 |
| $Arg_{16}$:$H^{\beta 2}$–$Tyr_{17}$:$H^N$ | 0.369 | 0.407 | 0.319 | 0.388 | 0.354 |
| $Arg_{16}$:$H^{\beta 3}$–$Tyr_{17}$:$H^N$ | 0.338 | 0.411 | 0.407 | 0.346 | 0.345 |
| $Tyr_{17}$:$H^\alpha$–$Arg_{18}$:$H^N$ | 0.254 | 0.241 | 0.244 | 0.242 | 0.244 |
| $Arg_{18}$:$H^{\beta 3}$–$Arg_{19}$:$H^N$ | 0.700 | 0.438 | 0.430 | 0.409 | 0.435 |
| $Arg_{19}$:$H^\alpha$–$Cys_{20}$:$H^N$ | 0.245 | 0.219 | 0.219 | 0.217 | 0.216 |
| $Arg_{19}$:$H^{\beta 2}$–$Cys_{20}$:$H^N$ | 0.382 | 0.433 | 0.417 | 0.433 | 0.436 |
| $Cys_{20}$:$H^\alpha$–$Trp_{21}$:$H^N$ | 0.247 | 0.249 | 0.225 | 0.285 | 0.359 |
| $Cys_{20}$:$H^{\beta 2}$–$Trp_{21}$:$H^N$ | 0.482 | 0.251 | 0.302 | 0.260 | 0.345 |
| $Cys_{20}$:$H^{\beta 3}$–$Trp_{21}$:$H^N$ | 0.326 | 0.253 | 0.412 | 0.246 | 0.241 |

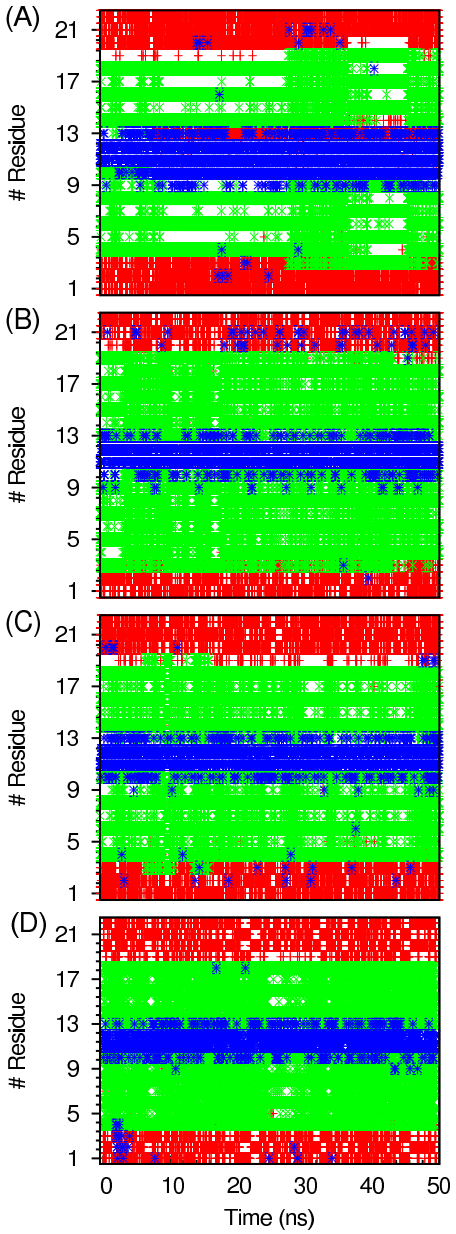


Figure 1: Time evolution of secondary structure assignement (STRIDE) of arenicin-2 sequence in A) M1, B) M3, C) 310K and D) c14 trajectories. Assignements are colored: red for coil, green for strand and blue for turn.